Macromolecular Rapid Communications
www.mrc-journal.de

Enhancing Passive Radiative Cooling Films with Hollow Yttrium-Oxide Spheres Insights from FDTD Simulation

Jeehoon Yu, Chanil Park, Byeongjin Kim, Sohyeon Sung, Hyun Kim, Jaeho Lee, Yong Seok Kim, and Youngjae Yoo**

Passive daytime radiative cooling (PDRC) presents a promising avenue for efficient thermal management without relying on electrical power. In this study, the potential of integrating Hollow Yttrium-Oxide Spheres (HYSs) within a Polydimethylsiloxane (PDMS) matrix to enhance PDRC is investigated. Through a combination of experimental characterization and computational analysis, the optical properties and radiative cooling performance of PDMS films embedded with HYSs are evaluated. These results demonstrate that HYSs significantly improve both solar reflectivity and long-wave infrared (LWIR) emissivity of the PDMS matrix. Finite-Difference Time-Domain (FDTD) simulations confirm the scattering efficiency of HYSs across various wavelength ranges, highlighting their effectiveness as additives for enhancing the radiative properties of passive cooling materials. Experimental validation reveals enhanced reflectivity and emissivity of PDMS films with embedded HYSs, resulting in superior cooling performance compared to non-HYS counterparts. Overall, this study underscores the potential of HYS-infused PDMS films as a promising solution for passive radiative cooling, with broad applicability in diverse domains requiring efficient thermal management solutions. Additionally, these research insights pave the way for establishing an AI database for passive radiative cooling research, offering new avenues for further exploration and application in this field.

1. Introduction

The Earth absorbs solar radiation and reaches thermal equilibrium by releasing the absorbed heat as long-wave infrared radiation through the atmospheric window, allowing heat to escape into outer space.[1] Thus, the thermal equilibrium on Earth is maintained through the emission of the absorbed heat through the atmospheric window, covering wavelengths between 8 and 13 μm.[2] Passive daytime radiative cooling (PDRC) refers to the emission of radiative energy, manifested as electromagnetic waves, occurring directly under sunlight.[3] Materials designed for PDRC inhibit the warming of spaces and objects without relying on electrical power. In contrast to traditional air-conditioning systems, structures treated with PDRC materials can achieve interior cooling without electricity.[4,5] Consequently, PDRC has emerged as a promising strategy for efficient heat management in various applications, such as buildings, where it can reduce cooling costs by reflecting solar radiation; vehicles, where it can lower internal temperatures and improve fuel efficiency; and energy storage systems (ESS), where it aids in maintaining optimal thermal conditions for improved battery performance.[6,7]

The performance of daytime radiative cooling depends on various factors. A representative factor is the high emissivity in the long-wave infrared (LWIR) range, which facilitates effective thermal radiation through the atmospheric window. This window is characterized by nearly ideal total atmospheric transmittance, attributable to

J. Yu, B. Kim, Y. Yoo
Department of Advanced Materials Engineering
Chung-Ang University
Anseong 17546, Republic of Korea
E-mail: yjyoo@cau.ac.kr

The ORCID identification number(s) for the author(s) of this article can be found under https://doi.org/10.1002/marc.202400770

DOI: 10.1002/marc.202400770

C. Park
Missile Research Institute-3rd Directorate
Agency for Defense Development
Daejeon 34186, Republic of Korea

S. Sung, H. Kim
Advanced Materials Division
Korea Research Institute of Chemical Technology
Daejeon 34114, Republic of Korea

J. Lee
Department of Mechanical and Aerospace Engineering
University of California
Irvine, CA 92617, USA

Y. S. Kim
Department of Chemistry
Sejong University
Seoul 05006, Republic of Korea
E-mail: yongskim@sejong.ac.kr

minimal absorption by atmospheric molecules (H_2O, CO_2, and O_2) within the 8–13 μm wavelength spectrum.[8] According to Kirchhoff's law of thermal radiation, the radiative emission of a body is equivalent to its absorptive capacity under thermodynamic equilibrium.[9] Consequently, to attain substantial electromagnetic emission within the infrared atmospheric window, materials with strong absorptive properties in the LWIR region must be used.[10]

Increased reflectiveness in visible and near-infrared (NIR) regions can suppress the surface heating of objects exposed to sunlight.[11] Considerable research efforts have been dedicated to the enhancement of LWIR emissivity using metamaterials, including photonic crystals and dielectric materials. Photonic structures, especially those made of polar dielectrics, have been used to enhance thermal emission in the atmospheric window by leveraging optically active resonances.[12] Furthermore, to attain heightened solar reflectivity, a layer of Ag has been introduced at the base of metamaterial structures.[13] Yao et al. noted that microspheres coated with resonating polar dielectrics exhibit an infrared emissivity of 0.93 and deliver a radiative cooling power of 93 W/m^2.[14] In our pursuit of effective PDRC coatings, we explored the use of yttrium-oxide (Y_2O_3) microspheres randomly dispersed within a polymer matrix.

Notably, hollow spheres embedded in a polymer matrix are promising materials for radiative cooling, owing to their significant solar reflectivity.[14,15] When exposed to sunlight, hollow spherical materials undergo non-interfering scattering, and multiple boundary interfaces enhance the diffusion of scattered light.[16] For example, porous polymers have been noted to exhibit improved solar reflectivity and radiative cooling efficacy even without an Ag coating. This enhancement is attributable to the porous nature of the coating layer, which helps amplify light scattering.[12,17–19] Recently, the development of straightforward and scalable coating techniques has emerged as a critical requirement for the commercial success of PDRC technologies. Consequently, researchers are actively exploring eco-friendly and uncomplicated coating methods based on boundary scattering, e.g., by leveraging hollow spheres and porous structures.[15] In this context, materials designed for passive radiative cooling by exploiting the scattering properties of hollow spheres offer excellent optical characteristics with lightweight films that can be efficiently applied to diverse structures through wet-coating techniques.[20,21] However, previous studies have not conclusively correlated the surface structure of hollow microspheres with their effectiveness in radiative cooling.

In our research, we embedded Hollow Yttrium-Oxide Spheres (HYSs) within a Polydimethylsiloxane (PDMS) matrix to improve both solar reflectivity and Long-Wave Infrared (LWIR) emissivity. Detailed studies were conducted to elucidate the impact of the surface morphology of these hollow spheres on their performance in radiative cooling. We hypothesized that the diffuse reflection of light from the rough surfaces of hollow spheres is more pronounced compared with that associated with their smooth counterparts. To validate this hypothesis, we minimized experimentation by employing FDTD simulation for optical analysis of materials, and analyzed the optical properties in radiative cooling through simulation, thus envisioning the advancement of passive radiative cooling through computer science. Additionally, micrometer-sized hollow spheres with both smooth and uneven surfaces were fabricated using melamine formaldehyde (MF) spheres as disposable templates. The hollow structure of the HYSs was achieved by adsorbing Y_2O_3 nanoparticles onto the uneven surfaces of the MF spheres through the Stöber process.[22] The enhanced solar reflectivity of HYSs was noted to enhance the daytime cooling performance of polymer matrices in PDRC materials. Outdoor field experiments highlighted the efficacy of the HYS films as radiative cooling agents for energy management. These films could reduce the temperature by an average of 9.8 °C below the ambient temperature, positioning them as viable alternatives for passive radiative cooling applications.

2. Results and Discussion

2.1. Preparation of Hollow Y_2O_3 Microspheres

Figure 1 illustrates the synthesis procedure and morphologies of the HYSs. The Y_2O_3 hollow structure was obtained using MF spheres as sacrificial templates owing to their uniform diameter.[23] Moreover, a urea precipitation method was used to obtain the MF@Y(OH)CO_3 core/shell microspheres.[24,25] The SEM image (Figure 1c) shows that the Y(OH)CO_3 nanoparticles adsorbed onto the smooth surface of the MF spheres with an average diameter of ≈2 μm (**Figure 2a**). The morphology of the Y(OH)CO_3 shell was influenced by the Y^{3+} concentration. During the formation of the core/shell structure, when the $Y(NO_3)_3$ concentration was 5 mmol g^{-1} (per 1 g MF), the Y(OH)CO_3 shell was not dense and exhibited a porous structure (Figure S2, Supporting Information). When 8 mmol g^{-1} of $Y(NO_3)_3$ was used, a raspberry-like Y(OH)CO_3 shell was observed, and the rough surface was expected to facilitate light scattering. The MF core templates were removed through calcination, yielding the HYSs (Figure 1d). The TEM images confirmed the achievement of a well-defined Y_2O_3 hollow structure.

Qualitative analysis was performed to more comprehensively characterize the Y_2O_3 hollow structure. The FTIR spectra of the as-prepared MF and MF@Y(OH)CO_3 microspheres revealed characteristic bands of MF. The absorption bands at 1540–1345, 1060, 1000, and 811 cm^{-1} were attributable to the vibrations of amino (—NH_2), ether (C—O—C), hydroxyl (—OH), and C—N—C groups, respectively.[24,26] After calcination, the MF absorption bands disappeared, and an absorption peak associated with Y–O stretching appeared at 556 cm^{-1}, as observed in the FTIR spectrum of the HYSs (Figure 2b).[27] The calcination process removed the MF templates and converted the Y(OH)CO_3 precursor to crystalline Y_2O_3. TGA results indicated that the thermal decomposition of MF initiated above ≈400 °C and was nearly complete at 650 °C. Conversely, the TGA curve of the HYSs indicated only a minor decrease in weight owing to the evaporation of physically adsorbed water. Therefore, when the MF@Y(OH)CO_3 core–shell microspheres were subjected to calcination at 800 °C for 2 h, the MF templates were effectively removed, yielding well-defined Y_2O_3 hollow structures. In addition, XRD results demonstrated that the calcination process yielded HYSs with high crystallinity. Calcined Y_2O_3 exhibited a strong peak (222) at 2θ = 29.2°, indicating the crystallite size, as shown in Figure 2d.[28]

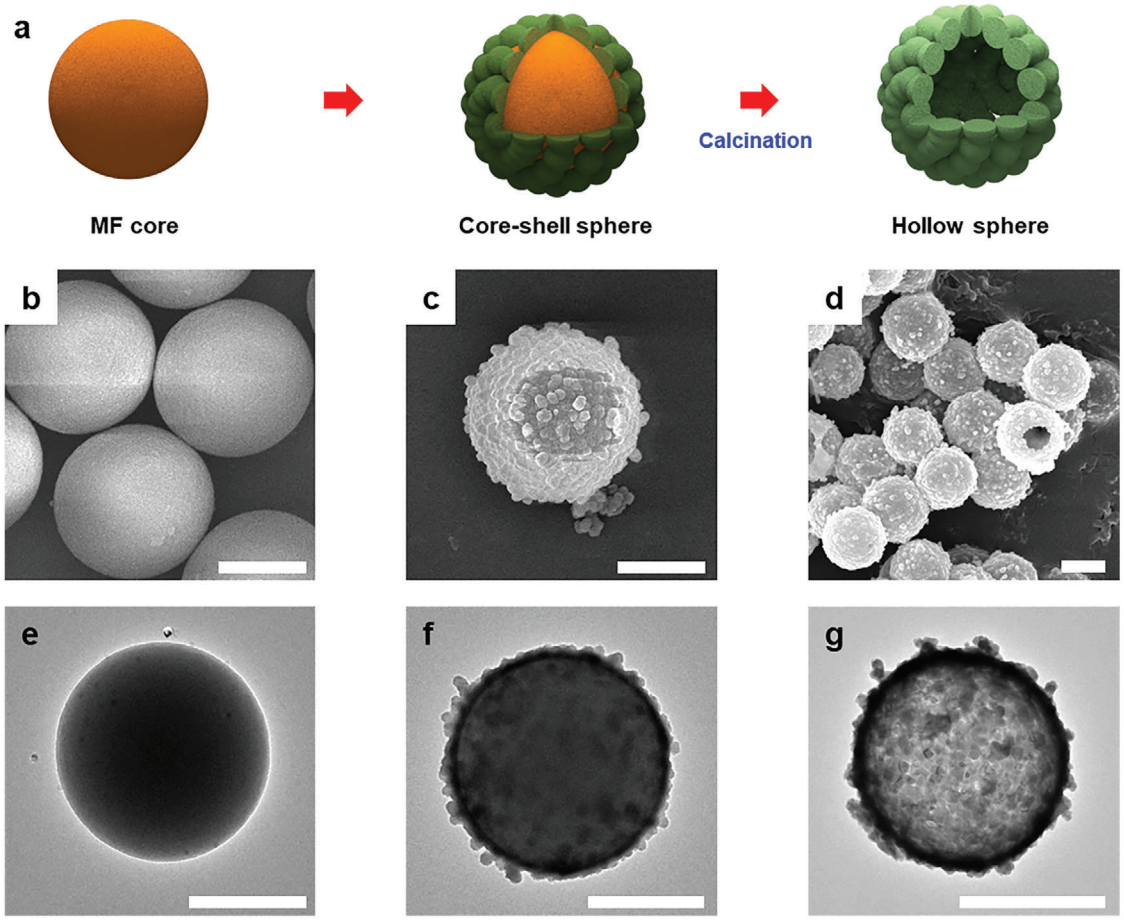

Figure 1. a) Schematic of the preparation of hollow Y_2O_3 microspheres using a scrificial template method. SEM images (middle) and TEM images (bottom) of the b,e) MF sphere, c,f) MF@Y(OH)CO_3 core/shell sphere, and d,g) hollow Y_2O_3 sphere (Scale bar: 1 μm).

2.2. Simulating the Optical Properties of HYSs Films Through Finite-Difference Time-Domain Method

We have engineered a novel PDRC coating, integrating highly reflective hollow yttrium oxide spheres (HYSs) into a PDMS (Polydimethylsiloxane) matrix. Our initial conjecture, drawn from observations depicted in Figure S3b (Supporting Information), hypothesized that the porous structure of HYSs could significantly enhance the reflection of light. To validate this hypothesis and explore the potential implications for our passive radiative cooling system, we conducted an exhaustive analysis. Utilizing finite-difference time-domain simulations, we systematically investigated three distinct models of HYSs: HYSs with a diameter of 2 μm, solid yttrium oxide spheres, and pre-assembled nano yttrium oxide spheres with a diameter of 200 nm, as delineated in **Figure 3d**.

Our FDTD simulation results, depicted in Figure 3a–c, elucidate that HYSs exhibited notable scattering efficiency within the spectral range of 1.2–2.8 μm, spanning the entirety of the visible and near-infrared spectrum. This is in contrast to the solid yttrium oxide spheres, which demonstrated lower scattering efficiency due to the lack of internal boundaries, particularly at shorter wavelengths. Notably, the presence of well-defined sine curves indicates the efficient realization of backscattering phenomena by these spheres. Conversely, solid yttrium oxide spheres demonstrated suboptimal scattering efficiency within the spectral range of 0–0.2, particularly in the ultraviolet and shorter visible wavelength regions. Pre-assembled nano yttrium oxide spheres exhibited promising scattering efficiency primarily within the wavelength range of 0–0.5 μm, with minimal efficacy observed elsewhere across the spectrum. These findings underscore the potential of HYSs as effective additives for enhancing the radiative properties of passive cooling materials. Furthermore, as shown in Figure 3e, the PDMS matrix induced radiation owing to the impedance mismatch caused by the sudden change in the refractive index within the atmospheric window region (8–13 μm), demonstrating the suitability of PDMS as an excellent polymer matrix for PDRC. This phenomenon not only underscores the intrinsic compatibility of PDMS with radiative cooling strategies but also accentuates its potential for diverse applications demanding precise thermal management. By effectively inducing radiation within this spectral range, PDMS emerges as a versatile and robust polymer matrix, with applications ranging from passive cooling systems to optoelectronic devices. In optoelectronic devices, PDMS is used for LED packaging to manage heat without compromising optical performance, in

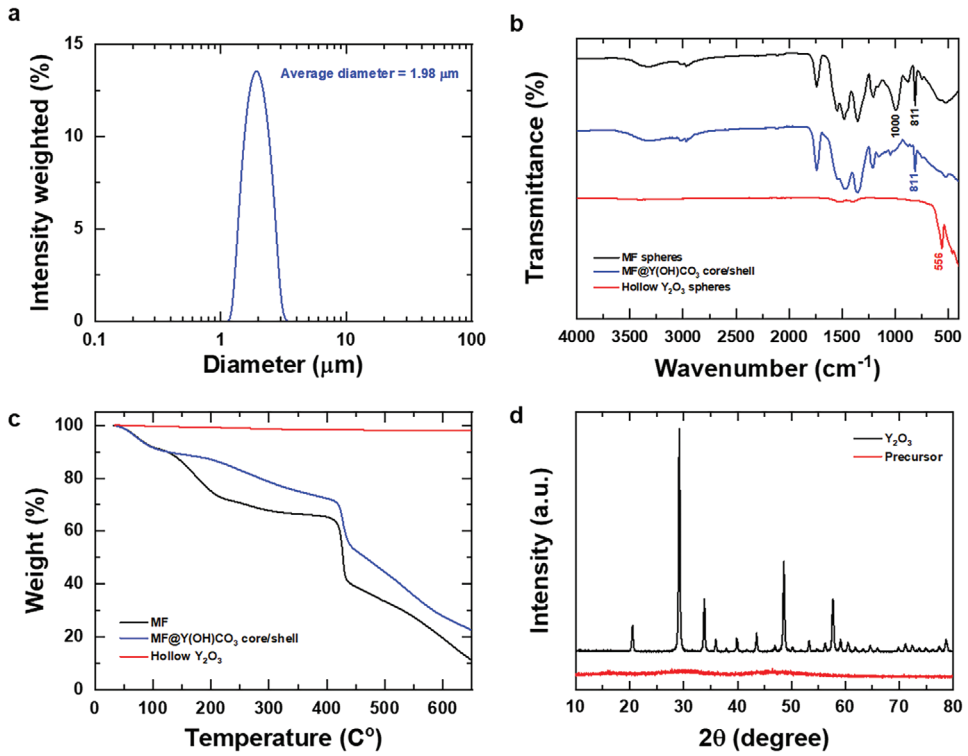

Figure 2. a) DLS size distribution and average diameter of the MF microspheres. b) FTIR spectra and c) TGA results of the MF microspheres, MF@Y(OH)CO_3 core/shell spheres, and HYSs. d) XRD patterns of the Y(OH)CO_3 precursor and HYSs.

flexible displays to provide transparency and thermal stability, and in optical sensors as a protective layer that ensures signal transmission and environmental resistance.[29]

To further investigate the synergy between the filler and the matrix, we applied each yttrium oxide filler into the PDMS matrix and conducted experiments as shown in Figure 3f. The modeling setup was as follows:

Light source: 0.2–2.5 μm wavelength

Source type: Planewave

We simulated the reflectivity across the UV–vis–NIR spectrum by constructing a unit of the passive radiative cooling material. As illustrated in Figure 3g, the hollow yttrium oxide spheres, due to their assembly from nano-sized particles, exhibited superior reflectivity compared to solid yttrium oxide spheres in the 0–0.5 μm range. Moreover, they demonstrated a uniquely high reflectivity in the 0.5–1 μm range, which is likely attributed to their hollow particle structure. Across other spectral ranges, they also showed the most consistent reflectivity, indicating the potential of this passive radiative cooling material to reflect solar energy effectively, especially in the UV region, which is a critical heating point. The material also maintains good reflectivity across other spectral regions, further proving its viability as a passive radiative cooling solution.

2.3. Optical Properties of HYS Films

Utilizing Finite-Difference Time-Domain (FDTD) simulations, the optical characteristics of the HYS film were validated. To elucidate how these simulated optical features manifest in practical scenarios, films incorporating well-dispersed HYSs within PDMS were meticulously fabricated and subjected to comprehensive optical measurements, as delineated in the cross-sectional views of **Figure** 4a–c. As delineated in Figure 4d, the HYS-infused film demonstrates significantly augmented reflectance in contrast to its pristine PDMS counterpart, with reflectance escalating commensurately with filler content. This pronounced enhancement underscores the efficient light scattering facilitated by the porous architecture inherent to HYSs. Furthermore, a thorough investigation into the emissivity of the HYS film across the visible and infrared spectra (wavelength range: 0.4–16 μm) was conducted. Emissivity, regarded equivalently to absorptivity as per Kirchhoff's radiation law (ϵ = 1–reflectivity–transmissivity),[8] was meticulously scrutinized. Notably, the HYS film exhibited a discernibly elevated emissivity in the long-wave infrared (LWIR) region, surpassing that of the pristine PDMS film (Figure 4e). This augmentation underscores the potential utility of HYS-infused materials in applications necessitating efficient thermal radiation modulation, such as thermal management systems and infrared shielding technologies.

2.4. Radiative Cooling Performance of HYS Films

The effectiveness of the HYS films in radiative cooling was assessed through outdoor experiments. The test setup was optimized to reduce non-radiative heat transfer, such as conduction

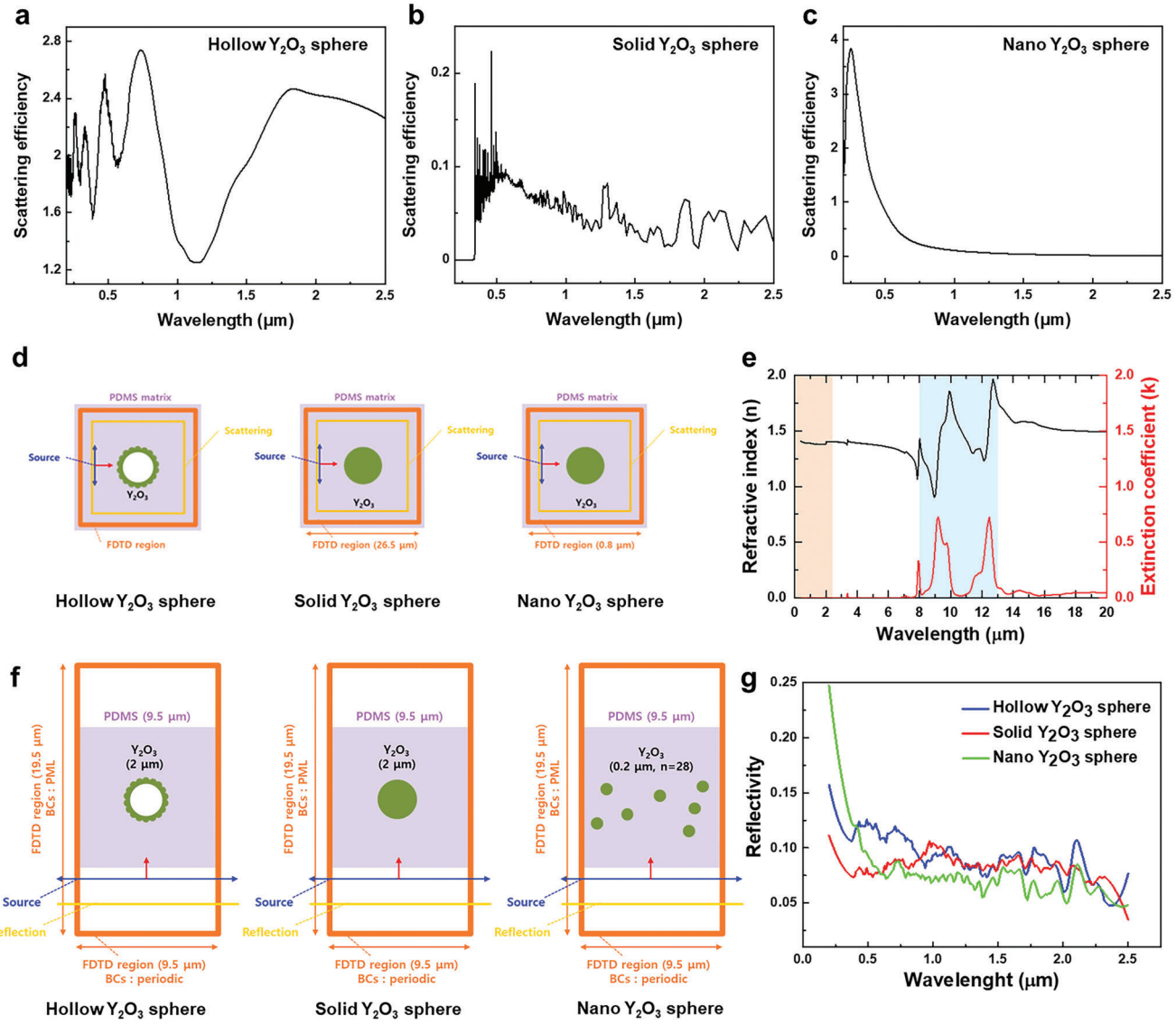

Figure 3. FDTD-simulated scattering efficiency of a) the hollow Y_2O_3 spheres, b) the solid Y_2O_3 spheres and c) the nano Y_2O_3 spheres. d) Schematic of FDTD simulation scattering efficiency modeling of hollow Y_2O_3 spheres, solid Y_2O_3 spheres, and nano Y_2O_3 spheres. e) Complex refractive index of the PDMS matrix. Black and red curves indicate the refractive index and extinction coeffcient, respectively. f) Schematic of FDTD simulation unit reflectivity modeling of hollow Y_2O_3 spheres, solid Y_2O_3 spheres, and nano Y_2O_3 spheres. g) Reflectivity simulation of hollow Y_2O_3 spheres, solid Y_2O_3 spheres, and nano Y_2O_3 spheres.

and convection, influenced by environmental elements such as wind and solar radiation. To prevent heat conduction from nearby roof structures, PDRC films with a thickness of 2 mm were placed on polystyrene (PS) foam blocks coated with an aluminum reflective layer (**Figure** 5b). The top of the PS enclosures was covered with an LDPE film to simplify the heat exchange dynamics against wind and weather changes. The wind-breaking feature of the LDPE film was crucial for analyzing the radiative transfer between the sample and ambient air.

Temperature variations near the samples within the experimental setup were continuously monitored using thermocouples attached to the underside of the PDRC films. Figure 5c,d shows the cooling performance of the HYS films and transparent PDMS films in outdoor settings in Daejeon, South Korea (latitude 36.39° N, longitude 127.36° E). The HYS films exhibited a pronounced cooling impact, validating our optical design approach (Figure 5a). Further examination of daytime temperature differentials between the samples and the environment showed that the HYS films maintained an average temperature ≈8.3 °C lower than the PDMS films without HYS. This result highlights the superior solar reflectivity of the HYSs and verifies their applicability as an efficient filler for PDRC. Additionally, the HYS films could reduce the temperature by an average of 9.8 °C below the ambient temperature during the day, underscoring their effectiveness as materials suitable for PDRC applications.

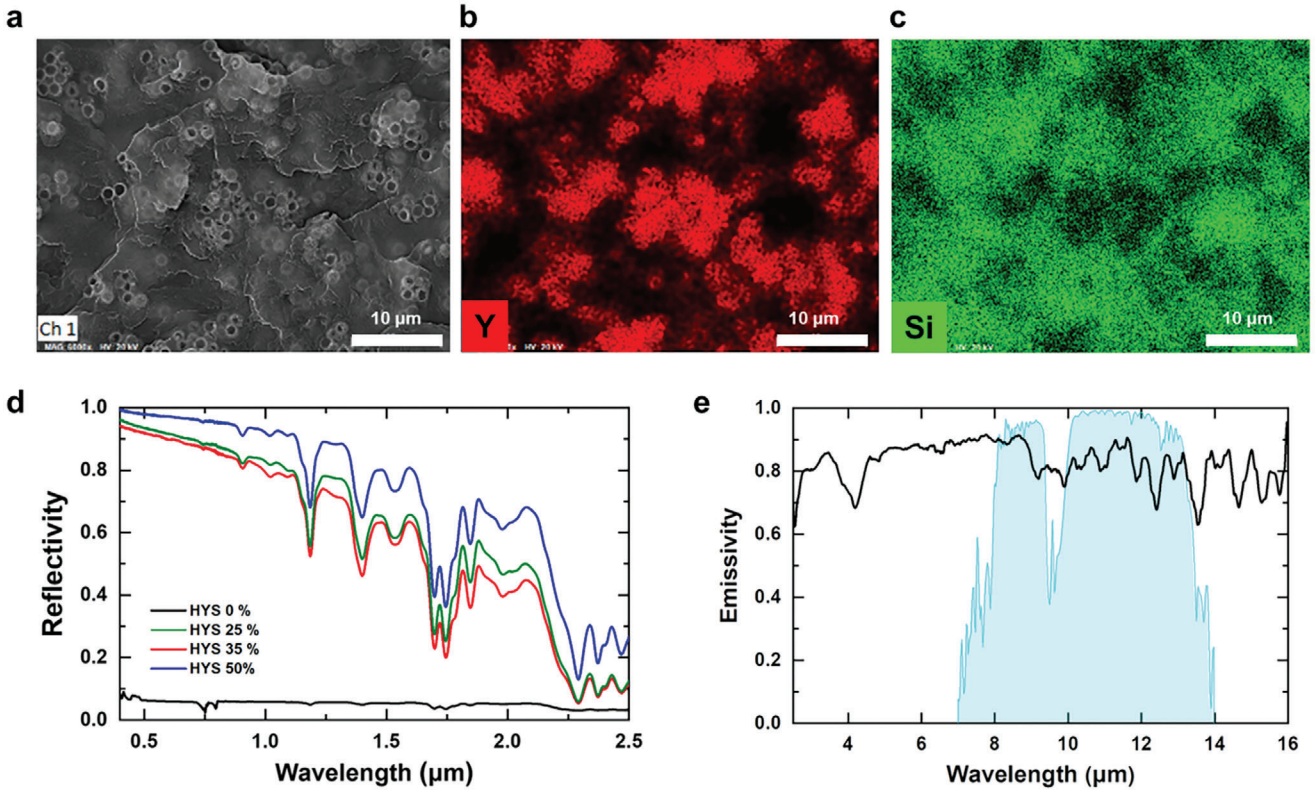

Figure 4. Cross-sectional a) SEM and b,c) EDS mapping images of the HYS film. d) Spectral reflectivity and e) LWIR emissivity of the clear PDMS and HYS films.

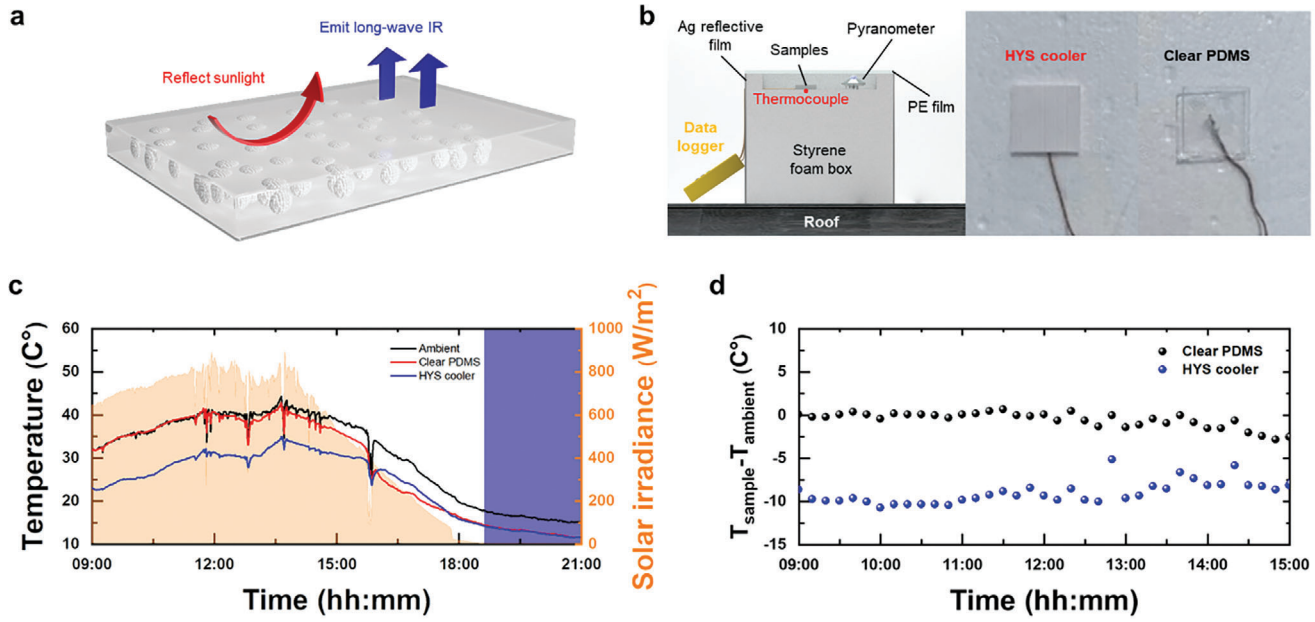

Figure 5. Radiative cooling performance. a) Schematic of the PDRC film using the HYSs. b) Schematic of the outdoor test setup and image of the samples during the outdoor experiments. Outdoor test results of the clear PDMS and HYS cooling films: c) temperature change and d) difference in ambient temperature and film surface temperature.

3. Conclusion

This study delves into the exploration of Hollow Yttrium-Oxide Spheres (HYSs) integrated within a Polydimethylsiloxane (PDMS) matrix to enhance Passive Daytime Radiative Cooling (PDRC). Through a fusion of experimental and computational analyses, we investigated the optical characteristics and radiative cooling efficacy of PDMS films embedded with HYSs. Our findings present compelling evidence that the incorporation of HYSs within the PDMS matrix markedly improves both solar reflectivity and Long-Wave Infrared (LWIR) emissivity. Leveraging Finite-Difference Time-Domain (FDTD) simulations, we validated the scattering efficiency of HYSs across diverse wavelength ranges, underscoring their potential as effective enhancers of the radiative properties of materials employed in passive cooling systems. Experimental validations corroborated the heightened reflectivity and emissivity of PDMS films augmented with HYSs, affirming the effectiveness of our optical design strategy. Furthermore, outdoor thermal measurements unveiled that HYS-infused films exhibit an average temperature differential ≈8.3 °C lower than non-HYS counterparts, thus showcasing superior cooling performance. In conclusion, our study elucidates the promising prospect of HYS-infused PDMS films as a solution for passive radiative cooling, with wide-ranging applicability across diverse domains necessitating efficient thermal management solutions. These research insights, facilitated by simulations, lay the groundwork for establishing an AI database for passive radiative cooling research, signaling prospective avenues for further exploration and application in this domain.

4. Experimental Section

Materials: Formaldehyde solution (37% in H_2O), melamine ($C_3H_6N_6$), sodium hydroxide (NaOH), formic acid (HCOOH, ≥ 98%), yttrium(III) nitrate hexahydrate ($Y(NO_3)_3{\cdot}6H_2O$), and urea (99–100%) were purchased from Sigma–Aldrich Co. (Korea) and used without further purification. PDMS (Sylgard 184) was purchased from Sewang Hightech (Seoul, Korea). Distilled deionized (DDI) water was used for all experiments.

Synthesis of Hollow Y_2O_3 Microspheres: MF core templates were synthesized by the polycondensation of melamine and formaldehyde molecules.[23,24] MF@$Y(OH)CO_3$ core/shell microspheres were prepared through urea precipitation, involving the following steps. The MF solution (2 w/v%) was sonicated for 1 min and stirred at 200 rpm to obtain a milky suspension. Next, 0.89 mmol urea and $Y(NO_3)_3$ (8 mmol g^{-1} for 1 g MF) were dissolved in the MF solution and stirred at 90 °C for 3 h. The core/shell spheres were separated from the suspension by centrifugation and washed several times with distilled water and ethanol. The white product was dried at 60 °C overnight and then calcined in air at 800 °C for 2 h.

Characterization: The microsphere morphology was analyzed through scanning electron microscopy (SEM, Mira 3LMU FEG, Tescan) at an accelerating voltage of 10 kV. The hollow structure of the microspheres was observed through transmission electron microscopy (TEM, FEI Talos F200X, Thermo Fisher Scientific). The surface morphologies of the microspheres were analyzed through atomic force microscopy (Nanoscope, Bruker). The size distribution of the MF spheres was determined through dynamic light scattering (Litesizer 500, Anton Paar). Fourier-transform infrared (FTIR) transmittance spectra of the microspheres were obtained using an FTIR instrument (Alpha-P, Bruker) operating in the attenuated total reflection mode. Thermal decomposition was observed through thermogravimetric analysis (TGA, TGA Q5000, TA Instrument) conducted in a nitrogen gas atmosphere at 20 °C min^{-1}. Yttrium oxide was characterized through X-ray diffractometry (XRD, Rigaku Ultima IV). The reflectance of the PDRC samples was measured in the wavelength range of 300–2500 nm, using a UV–Vis–NIR spectrometer (Cary 5000, Agilent Technologies) equipped with an integrating sphere (DRA-2500, Agilent Technologies). The reflectance and transmittance of the PDRC samples over the wavenumber range of 5000–400 cm^{-1} were determined using an FTIR spectrometer (Vertex 80v, Bruker) equipped with an integrating sphere (MCT, PIKE Technologies). Spectral emissivity values were determined using Kirchhoff's radiation law.[9,25]

Outdoor Thermal Measurements: Outdoor tests were conducted using a styrene foam box coated with aluminum Mylar tape to prevent radiation from surrounding the building. The top side of the styrene box was covered with an infrared transparent low-density polyethylene (LDPE) film to reduce convection (Figure S6, Supporting Information).[27,30] PDRC samples were placed on the styrene foam stage, and K-type thermocouples were attached to the bottom of the samples. Temperature changes were recorded using a multichannel data logger (PCE-T 1200, PCE Instruments UK Ltd.). The ambient temperature around the PDRC samples was measured. Solar irradiance was recorded using a pyranometer (Apogee Instruments, SP-510 solar system, and AT-100 microCache data logger). Outdoor experiments were conducted in Daejeon, South Korea, on November 8, 2021.

Supporting Information

Supporting Information is available from the Wiley Online Library or from the author.

Acknowledgements

This research was supported by the National Research Foundation of Korea (NRF) grants (No. 2023R1A2C1005459) and the Materials/Parts Technology Development Program (RS-2024-00421058) funded by the Ministry of Trade, Industry & Energy (MOTIE, Korea). This work was also supported by a Korea Institute for Advancement of Technology (KIAT) grant funded by the Korea Government (MOTIE) (P0012453, HRD Program for Industrial Innovation). This work was also supported by the faculty research fund of Sejong University in 2024.

Conflict of Interest

The authors declare no conflict of interest.

Data Availability Statement

The data that support the findings of this study are available from the corresponding author upon reasonable request.

Keywords

optical properties/techniques, nano-structures, hybrid, computational modelling, yttrium oxide

Received: October 1, 2024
Revised: October 18, 2024
Published online: October 30, 2024

[1] C. Park, C. Park, J.-H. Choi, Y. Yoo, *Elastomers Compos.* **2022**, *57*, 62.

[2] S. Gamage, D. Banerjee, M. d. M. Alam, T. Hallberg, C. Åkerlind, A. Sultana, R. Shanker, M. Berggren, X. Crispin, H. Kariis, D. Zhao, M. P. Jonsson, *Cellulose* **2021**, *28*, 9383.
[3] X. Li, J. Peoples, Z. Huang, Z. Zhao, J. Qiu, X. Ruan, *Cell Rep. Phys. Sci.* **2020**, *1*, 100221.
[4] T. Wang, Y. Wu, L. Shi, X. Hu, M. Chen, L. Wu, *Nat. Commun.* **2021**, *12*, 365.
[5] G. J. Lee, Y. J. Kim, H. M. Kim, Y. J. Yoo, Y. M. Song, *Adv. Opt. Mater.* **2018**, *6*, 1800707.
[6] T. Wang, Y. Zhang, M. Chen, M. Gu, L. Wu, *Cell Rep Phys Sci* **2022**, *3*, 100782.
[7] T. Li, Y. Zhai, S. He, W. Gan, Z. Wei, M. Heidarinejad, D. Dalgo, R. Mi, X. Zhao, J. Song, J. Dai, C. Chen, A. Aili, A. Martini, R. Yang, J. Srebric, X. Yin, L. Hu, *Science* **2019**, *364*, 760.
[8] M. Chen, D. Pang, X. Chen, H. Yan, Y. Yang, *EcoMat* **2022**, *4*, e12153.
[9] G. Kirchhoff, *Ann. Phys.* **1860**, *185*, 275.
[10] H. Zhong, P. Zhang, Y. Li, X. Yang, Y. Zhao, Z. Wang, *ACS Appl. Mater. Interfaces* **2020**, *12*, 51409.
[11] D. Chae, S. Son, Y. Liu, H. Lim, H. Lee, *Adv. Sci.* **2020**, *7*, 2001577.
[12] M. Lee, G. Kim, Y. Jung, K. R. Pyun, J. Lee, B.-W. Kim, S. H. Ko, *Light Sci Appl* **2023**, *12*, 134.
[13] Y. Zhang, X. Chen, B. Cai, H. Luan, Q. Zhang, M. Gu, *Adv. Photonics Res.* **2021**, *2*, 2000106.
[14] Y. Zhai, Y. Ma, S. N. David, D. Zhao, R. Lou, G. Tan, R. Yang, X. Yin, *Science* **2017**, *355*, 1062.
[15] D. Li, X. Liu, W. Li, Z. Lin, B. Zhu, Z. Li, J. Li, B. o. Li, S. Fan, J. Xie, J. Zhu, *Nat. Nanotechnol.* **2021**, *16*, 153.
[16] J. Song, W. Zhang, Z. Sun, M. Pan, F. Tian, X. Li, M. Ye, X. Deng, *Nat. Commun.* **2022**, *13*, 4805.
[17] B. o. Xiang, R. Zhang, Y. Luo, S. Zhang, L. Xu, H. Min, S. Tang, X. Meng, *Nano Energy* **2021**, *81*, 105600.
[18] A. Leroy, B. Bhatia, C. C. Kelsall, A. Castillejo-Cuberos, M. H. Di Capua, L. Zhao, L. Zhang, A. M. Guzman, E. N. Wang, *Sciences Adv.* **2019**, *5*, eaat9480.
[19] X. Zhang, *Science* **2017**, *355*, 1023.
[20] Y. Chen, J. Mandal, W. Li, A. Smith-Washington, C.-C. Tsai, W. Huang, S. Shrestha, N. Yu, R. P. S. Han, A. Cao, Y. Yang, *Sciences Adv.* **2020**, *6*, eaaz5413.
[21] W. Xie, C. Xiao, Y. Sun, Y. Fan, B. Zhao, D. Zhang, T. Fan, H. Zhou, *Adv. Funct. Mater.* **2023**, *33*, 2305734.
[22] W. Stober, A. Fink, E. Bohn, *J. Colloid Interface Sci.* **1968**, *26*, 62.
[23] I. W. Cheong, J. S. Shin, J. H. Kim, S. J. Lee, *Macromol. Res.* **2004**, *12*, 225.
[24] Y. Wu, Y. Li, L. Qin, F. Yang, D. Wu, *J. Mater. Chem. B* **2013**, *1*, 204.
[25] A. P. Raman, M. A. Anoma, L. Zhu, E. Rephaeli, S. Fan, *Nature* **2014**, *515*, 540.
[26] B. Friedel, S. Greulich-Weber, *Small* **2006**, *2*, 859.
[27] T. Li, Y. Zhai, S. He, W. Gan, Z. Wei, M. Heidarinejad, D. Dalgo, R. Mi, X. Zhao, J. Song, J. Dai, C. Chen, A. Aili, A. Vellore, A. Martini, R. Yang, J. Srebric, X. Yin, L. Hu, *Science* **2019**, *364*, 760.
[28] G. Jia, M. Yang, Y. Song, H. You, H. Zhang, *Cryst. Growth Des.* **2009**, *9*, 301.
[29] J. P. Bijarniya, J. Sarkar, P. Maiti, *Sci. Rep.* **2021**, *11*, 893.
[30] D. Chae, M. Kim, P.-H. Jung, S. Son, J. Seo, Y. Liu, B. J. Lee, H. Lee, *ACS Appl. Mater. Interfaces* **2020**, *12*, 8073.

